

Scattering of VHF radio waves from within the top 700 m of the Antarctic ice sheet and its relation to the depositional environment: a case-study along the Syowa–Mizuho–Dome Fuji traverse

SHUJI FUJITA,¹ HIDEO MAENO,² TERUO FURUKAWA,³ KENICHI MATSUOKA⁴

¹Department of Applied Physics, Graduate School of Engineering, Hokkaido University, Sapporo 060-8628, Japan

²Communications Research Laboratory, Nukui-kita, Koganei, Tokyo 184-8795, Japan

³National Institute of Polar Research, Kaga, Itabashi-ku, Tokyo 173-8515, Japan

⁴Institute of Low Temperature Science, Hokkaido University, Sapporo 060-0819, Japan

ABSTRACT. Radio-wave scattering is a convenient method to image the properties of large internal regions of ice sheets. We used a ground-based radar system with short pulses of 60 and 179 MHz frequencies to scatter off internal strata within 100–700 m of the surface in the ice sheet of East Antarctica. Data were examined along an 1150 km long traverse line that was approximately along the ice flowline from inland of Dome Fuji station to the coast. The scattered waves are from strata, and the dominant cause of the scattering was changes in dielectric permittivity across the strata. Therefore, density fluctuations primarily cause the scattering, although variations in ice-crystal fabrics and acidity could also have effects. The power scattered from the same depths varied by > 15 dB from one location to another. These variations correlate with the accumulation rate, changes in the surface slope, and subglacial bedrock undulations. Variations of the scattered power suggest that density contrasts in the strata are highly variable depending on these interdependent local conditions. The distribution of strata along the route allowed estimates of the ice-flow trajectories to depths of about 250 m.

INTRODUCTION

Understanding the physical structure of the Antarctic ice sheet is important for determining how this huge ice mass responded to past climate change and how it will respond to present and future climate changes. The radar-sounding method has proved to be a powerful tool for investigating the subsurface structure of large ice masses: over the last few decades, a wide range of radio to microwave frequencies from a few MHz to a few GHz have been successfully used to image the ice structure (e.g. Robin and others, 1969; Bogorodsky and others, 1985). Recent efforts have been made to develop modern ice-sounding radars (e.g. Gogineni and others, 1998; Nixdorf and others, 1999; Uratsuka and others, 2000; Matsuoka and others, 2002). Scattering of electromagnetic waves from the ice is caused by sudden changes in the complex dielectric permittivity of strata in ice sheets; thus the scattering is often treated as being from internal reflections. A number of researchers have investigated the origin of the sudden changes and identified three major causes of the sudden changes in the complex permittivity: changes in (1) density, (2) acidity and (3) crystal-orientation fabrics (Robin and others, 1969; Harrison, 1973; Gudmandsen, 1975; Paren and Robin, 1975; Clough, 1977; Ackley and Keliher, 1979; Millar, 1981; Robin and Millar, 1982; Moore, 1988; Fujita and Mae, 1994; Jacobel and Hodge, 1995; Fujita and others, 1999, 2000).

The current understanding is that the dominant reflection mechanism depends on the physical conditions within the ice

sheet, depth ranges and regions, and on the radar frequency (Fujita and Mae, 1994; Fujita and others, 1999, 2000). Thus, the dominant scattering mechanism needs to be discussed in terms of all these conditions. A scattering mechanism that dominates in the Antarctic ice sheet might not dominate in Greenland or vice versa, because essential conditions like

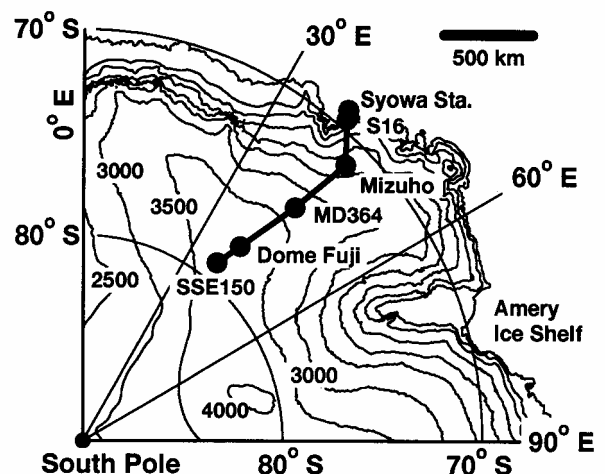


Fig. 1. Contour map of East Antarctica. The ice flow is normal to the contours. The measurements were done on the 1150 km long traverse route shown as the thick solid line. See Table 1 for further descriptions of the sites.

Table 1. Location of the major sites along the 1150 km long traverse

	Location	Elevation m a.s.l.	Distance from Dome F* km	Flow velocity [†] m a ⁻¹	Note
SSE150	78°41' S, 37°47' E	3722	157	No data	Southernmost point
Dome F	77°19' S, 39°42' E	3810	0	~ 0	Summit and ice-coring site
MD364	74°01' S, 43°00' E	3353	371	4.1	
Mizuho	70°42' S, 44°17' E	2250	738	22.2	
SI6	69°02' S, 40°03' E	585	993	5.2	Northernmost point

* Dome F is the distance origin because the data further south are incomplete, and because Dome F is located at the origin of ice flow.

[†] After Motoyama and others (1995).

temperature, impurity distributions and the depositional environment (e.g. accumulation rates) are different in the two ice sheets. This also applies to two different regions in the same ice sheet. Most studies have also paid insufficient attention to the effect of frequencies in discussing reflection mechanisms. In this study, the dependence of scattering on frequency is used to identify the scattering mechanisms.

This study complements a previous study (Fujita and others, 1999) that mapped the dominant internal reflection mechanisms using 60 and 179 MHz radar along the same route as that in this study. The route mapped is along an 1150 km long traverse line from SSE150 (3722 m a.s.l.) through Dome Fuji (hereafter Dome F), the second highest dome in East Antarctica (3810 m a.s.l.), to SI6 (585 m a.s.l.) on the coast (Fig. 1; Table 1). The previous study found four physically distinct zones in the ice sheet: P_D , P_{COF} , C_A and a basal echo-free zone. Here, P is permittivity, C is conductivity, and subscripts D, COF and A refer to density, crystal-orientation fabrics and acidity, respectively. The present study focuses on the top 700 m of the ice sheet. This was previously identified as the P_D zone where permittivity is most dependent on density.

In this paper, we examine the scattering in terms of the depositional environment at the surface of the ice sheet. We also examine how the scattering changes within the P_D zone with depth and location. This is important for interpreting the remote-sensing data that measure the shallow interior of the ice sheet using radio waves.

A number of glaciological investigations have been carried out along and near the 1150 km traverse line. Endo and Fujiwara (1973) measured snow density and other characteristics of the snow cover along a 2500 km long traverse in East Antarctica, from east Dronning Maud Land through Dome F to the South Pole. Their 2500 km traverse includes our 1150 km traverse. Long after their pioneering work, researchers investigated the characteristics of the snow cover in more detail along the 1150 km traverse to Dome F. These studies include accumulation-rate measurements (Satow and others, 1999), ice-thickness measurements (Maeno and others, 1994), snow-density measurements (Azuma and others, 1997; Fujita and others, 1998; Motoyama and others, 1999), surface velocity measurements (Motoyama and others, 1995) and surface micro-relief such as the distribution of sastrugi, dunes and thermal cracks (Furukawa and others, 1996). Based on these data from field surveys and the two-frequency radar data, this paper shows features of internal electromagnetic scatter and its relation to the surface features. In particular, it shows that the scattered signal at

160 m below the surface is high when the ice is thick, the surface is relatively flat and the accumulation rate is high.

EXPERIMENT

Basic radar equation

Here we outline the basic ideas for diagnosing scattering from within the ice sheet using radar (for more detail, see Fujita and others, 1999). The quantity measured by the receiver is a time series of received power. Therefore, we consider the dependence of the received power P_R on the transmitted power P_T , the timing of the signal that determines the depth z of the scattering event, the energy loss due to dielectric absorption L , and other factors that depend on the radar system. If the scatterers are distributed on strata within the ice, the scattering process can be approximated as Fresnel reflection. Then the radar equation for the radar placed on the ice-sheet surface is (e.g. Bogorodskiy and others, 1985)

$$P_R = \frac{P_T G^2 \lambda^2 q R}{64 \pi^2 z^2 L}, \tag{1}$$

where G , λ and q are, respectively, antenna gain, wavelength in vacuum, and refraction gain, the latter of which accounts for modification of the beamwidth by refraction at the air/ice interface. The physical properties of the ice at depth z are mostly contained in the power reflection coefficient, R , but partly in L . However, instead of using Equation (1) to estimate R , we maintain a constant P_T and evaluate the measured variations in P_R , because small uncertainties in L and possible systematic errors in G would cause uncertainties in R .

Table 2. Specifications of the two radar systems used in this experiment

	Frequency	60 MHz	179 MHz
Transmitter	Peak power	1 kW	1 kW
	Pulse width	250 ns	150 ns/350 ns
	Resolution in ice	21 m	13 m/30 m
	Wavelength in ice	2.8 m	0.94 m
	Sensitivity	-110 dBm*	-110 dBm
Receiver	Noise level	< 1 dB	< 1 dB
	Type	3-element Yagi	3-element Yagi
Antenna	Gain	7.2 dBi [†]	8.15 dBi
	Beamwidth	70°	70°

* dBm is a unit expressing power level in decibels with reference to a power of 1 mW.

[†] dBi is a unit for expressing antenna gain in decibels with reference to a power of an ideal isotropic antenna.

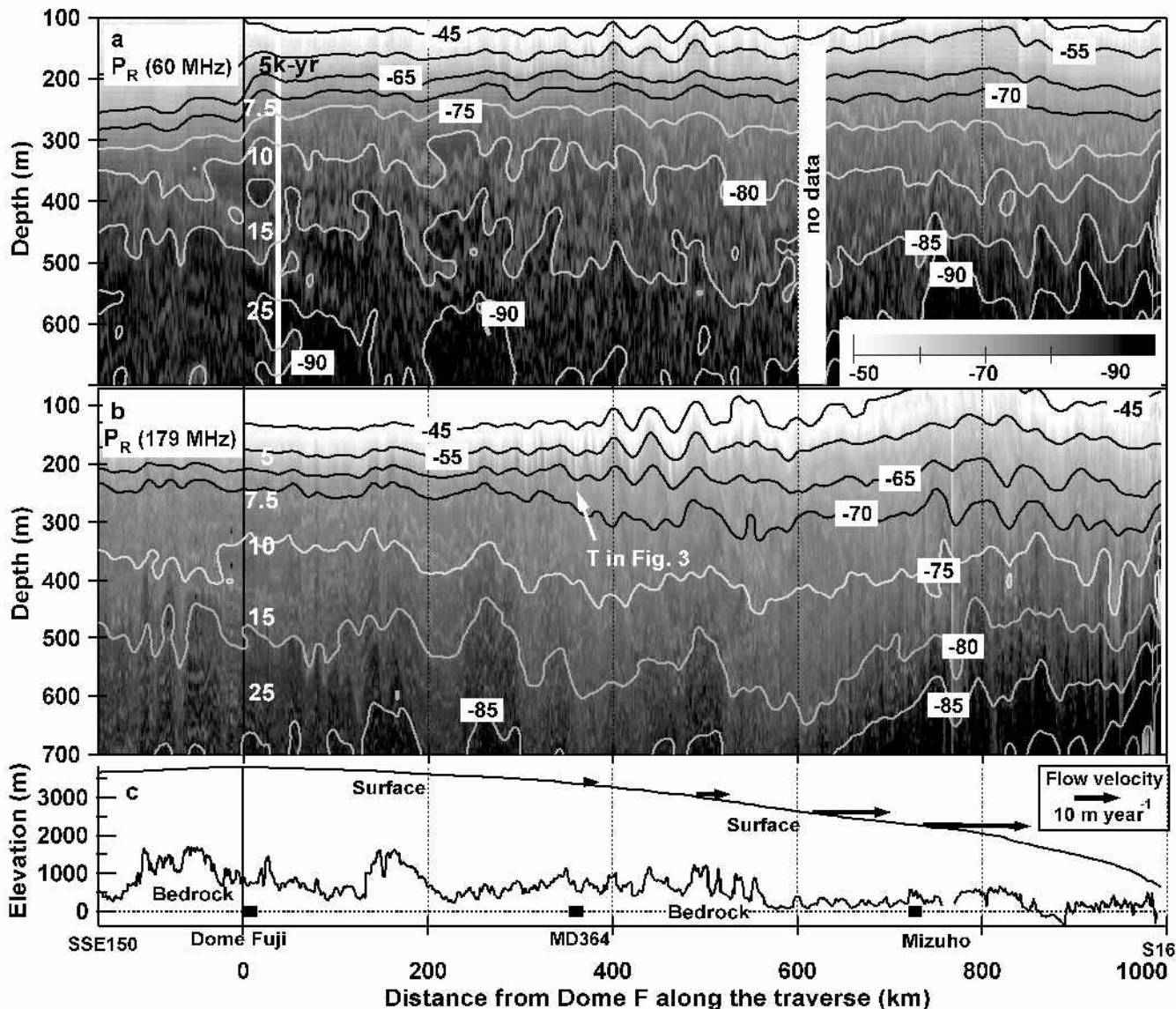


Fig. 2. Distribution of the received power, P_R (dBm) from within the top 100–700 m of the ice sheet along the 1150 km traverse. The upper two density plots are from the 60 MHz radar with a pulse width of 250 ns (upper) and from the 179 MHz radar with a pulse width of 150 ns (lower). A gray scale for the received power is shown at the upper right. The mean trends of uniform P_R are shown by contour lines. The 15 km running averages of uniform P_R are shown as contour lines. The contour interval is halved below the -65 contour. The 60 MHz data between SSE150 and Dome F and above 300 m were affected by internal noise of the radar system, i.e. the lowering of the contour lines in this region is an artifact. Instead, the P_R values should be several dB lower. Internal echoes from strata are often shown as the first derivative of the received power vs depth, but this is not done here because such a filtering process would have caused a loss of information on scattering strength. The age of ice is given at the coring site of Dome F (Watanabe and others, 1999). The bedrock elevation plot at the bottom indicates some correlation between peaks of the bedrock and near-surface contour peaks in P_R . Also shown is the surface elevation, ice-flow velocity and three locations that are imaged in finer detail in Figure 3. The surface elevations are from the European Remote-sensing Satellite-1 (ERS-1) satellite-borne radar altimeter, and the bedrock elevation was measured by the radar sounding.

The time-series variation of P_R was converted to values at each depth z using the radar wave speed in firn and ice. When we determine the specifications of the radar system, P_T , G , λ and q are fixed. In addition, the distance between the radar and the scattering region z adds a geometrical factor in Equation (1) due to spreading of the wave front. We assume $L = \exp(2\alpha z)$, where α (dB m $^{-1}$) is the attenuation coefficient. In the temperature range of inland Antarctica (-30° to -60°C) the attenuation coefficient for these radio waves is $6\text{--}2 \times 10^{-3}$ dB m $^{-1}$ according to an estimate of the dielectric absorption of ice containing acidity (Fujita and others, 2000). This is consistent with earlier radar measurements (e.g. Bogorodsky and others, 1985). Assuming the electro-

magnetic waves travel several hundred meters between radar and strata, the energy loss from dielectric absorption is only a few dB. Therefore, changes of P_R over a small depth range that is more than a few dB are most likely due to changes in R and thus indicate a change of some ice property.

Equation (1) assumes that the interfaces are smooth planes. Handling of the scattering component from an undulating surface or slightly rough surface is described in Fujita and others (1999).

Radar systems

The radar systems were mounted on two snow vehicles, one

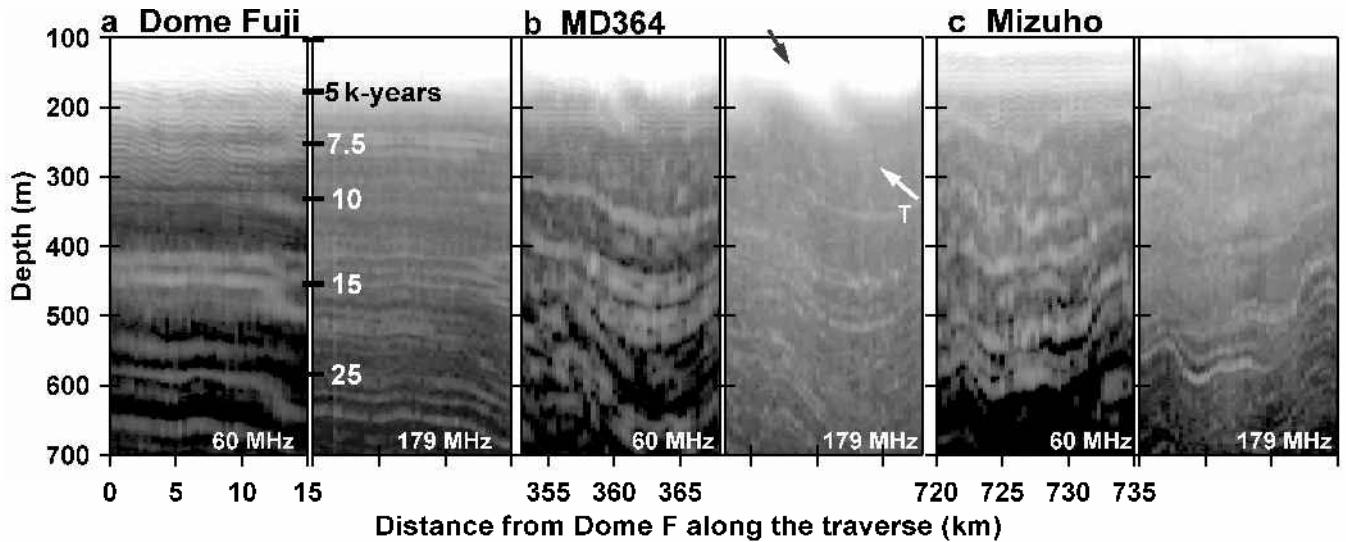


Fig. 3. Finer-scale features of the received power P_R along the three 15 km long cross-sections marked in Figure 2. Gray scales for the power are the same as in Figure 2. These density plots indicate continuity and stability of stratified structure of the scatterers near the dome summit compared with the downstream regions. The very thin striped interference pattern in the top 300 m of the 60 MHz data is due to internal noise of the radar system. The age of ice is given at the coring site of Dome F (Watanabe and others, 1999). The arrows labeled “T” indicate an example of the suggested trajectories.

for each frequency. The transmitting and receiving antennas were on opposite sides of the vehicle, and were kept parallel, 6.4 m apart. The centers of the antennas were 3.2 m above the ice-sheet surface. All the data were digitally recorded. To calibrate the received power, we regularly calibrated a relation between the power from the antenna and the output in the recording system. The specifications of the radar systems at 60 and 179 MHz are listed in Table 2. Both systems have the same transmission power (1 kW).

Observation sites and data sampling

The 1150 km traverse route began from a site located 150 km south of Dome F, went through both Dome F and Mizuho station, and reached the coast at SI6 (Fig. 1; Table 1). This route roughly follows the flowline except the section for 245 km north of Mizuho station. Dome F is located at the dome summit, hence it is the origin of the ice flow. The measurements were carried out from 1995 to 1997. During the traverse, the radio-echo data were continuously recorded, and the antennas were always oriented along the traverse line.

A two-frequency algorithm to distinguish radar reflection mechanisms

To determine physical properties in the ice, it is important to estimate the ice property that dominates the scattering at each depth. We used an algorithm that uses two frequencies to distinguish between scattering caused by permittivity changes P_D , P_{COF} and electrical conductivity changes C_A . The algorithm is based on the complex dielectric properties of ice Ih crystals. The frequency dependence of R will depend on whether the dominant scattering mechanism is permittivity or conductivity (Fujita and Mae, 1994; Fujita and others, 1999, 2000). An essential difference is that the power reflection coefficient due to changes in conductivity is inversely proportional to the square of the frequency, whereas the power reflection coefficient due to changes in permittivity is independent of the frequency. Therefore, if

two frequencies are used for radar sounding, the difference in P_R for the two frequencies depends on the scattering mechanism. Fujita and others (1999) used Equation (1) to estimate that permittivity-based reflections cause the difference of the P_R between the two frequencies ($\Delta P_R = P_R(f_2) - P_R(f_1)$ (dB)) to be about $10 \log_{10}(f_2/f_1)$ dB larger than that from conductivity-based reflections. In the present case, f_1 and f_2 are 60 and 179 MHz, respectively, so the magnitude of the change is about 9.5 dB. This value is a criterion to distinguish the permittivity- and conductivity-based reflections.

RESULTS

Large-scale distribution of the received power P_R

The large-scale distribution of P_R shows how the strata follow trends in snow accumulation, bedrock topography, surface slope and other characteristics of the ice-sheet environment. Figure 2 shows the distribution of the received power P_R from within the top 100–700 m of the ice sheet along the traverse. As a general trend, P_R for both frequencies decreases with depth because of increases in both depth z and loss factor L in Equation (1). The gray-scale images indicate that P_R generally has larger fluctuations and better feature contrast at 60 MHz, especially below about 250 m. In addition to the steady decrease of P_R with depth, P_R fluctuates along the traverse. At depths of 100–250 m, P_R fluctuates along the traverse with a length scale from a few km (in the raw gray-scale image) to about 30 km (in the mean trends indicated as the contour lines) and an amplitude that decreases with increasing depth. Deeper in the ice, P_R fluctuates along the traverse at a longer scale of 100 km shown as white contours; the amplitude of these contours increases with depth at some locations. From the data in Figure 2, we extracted the shallow fluctuations of P_R at 160 m depth along the traverse and plot them in Figure 5a and b (shown later). At 60 MHz, the fluctuations are within 5 dB at sites within 200 km of the dome, increase to about 10 dB at sites 200–700 km from the dome,

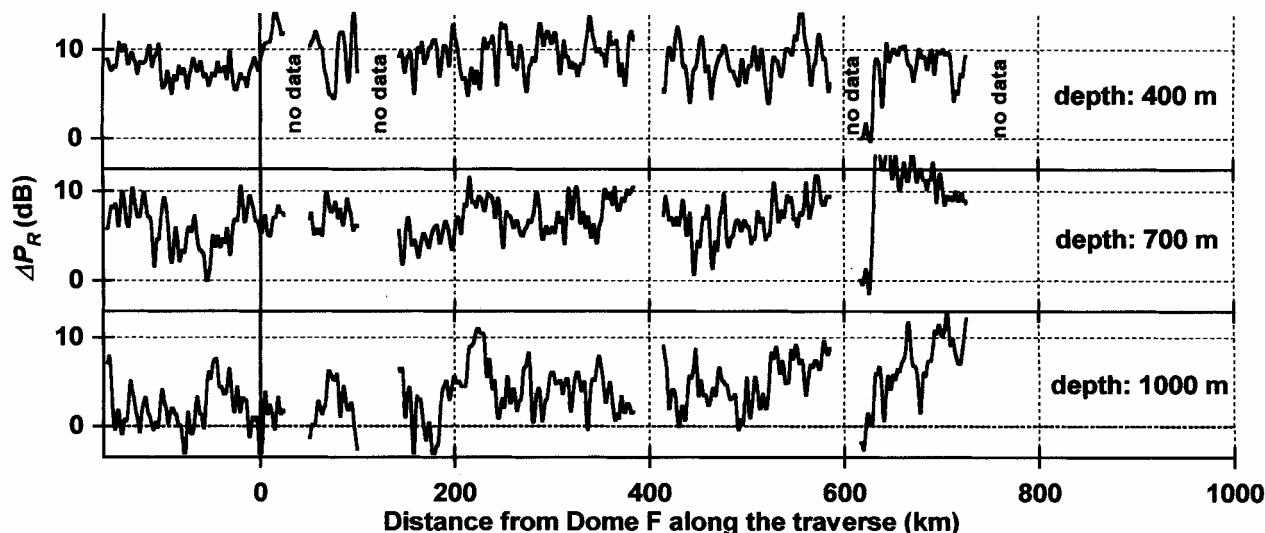


Fig. 4. Variation of $\Delta P_R = P_R(179 \text{ MHz}) - P_R(60 \text{ MHz})$ along the traverse for depths of 400, 700 and 1000 m. The 179 MHz radar used a pulse width of 350 ns. The dominant reflection mechanism is changes in dielectric permittivity when ΔP_R is close to 10 dB (Fujita and others, 1999), whereas the dominant reflection mechanism is changes in electrical conductivity when ΔP_R is close to 0 dB.

and finally decrease beyond 700 km. For 179 MHz the trend is the same, but the amplitude is larger between 400 and 700 km. These fluctuations seen in the gray-scale image penetrate from the surface into the ice sheet. However, they are traceable only down to 250 m.

The decrease of P_R with depth (dP_R/dz) also changes from one region to another and depends on frequency. At 60 MHz, the gradient (dP_R/dz) at depths above about 300 m changes only slightly with location, while at 179 MHz the gradient (dP_R/dz) at depths above about 300 m decreases at sites between 200 and 700 km. That is, as the location moves away from Dome F, the shallower P_R tends to decrease and the deeper P_R tends to increase. The average values of P_R are largest in the vicinity of the dome (see Fig. 5a and b, shown later), but this average tendency decreases by about 5–10 dB away from the dome.

Stratified features

Comparing the distribution of P_R over several small regions indicates how the continuity and stability of the strata changes from region to region. To observe the continuity of the stratified features, three 15 km long cross-sections marked in Figure 2c were extracted from the 1150 km cross-section of Figure 2. These are shown in Figure 3 on an expanded scale. The cross-section was measured near Dome F, near MD364 and near Mizuho (see Table 1). The continuity and horizontal uniformity of strata is clear in the vicinity of the dome summit. The strata remain visible but are more widely spaced and tilted further from Dome F. Because what we are observing by ice radar is interference patterns from many strata within a radar pulse (Moore, 1988; Jacobel and Hodge, 1995; Fujita and others, 1999), the distorted layer features indicate that the interference pattern changed from one place to another along a distance scale (along the traverse) of less than a few hundred meters. This interference effect is a complex function of depth and thickness of the strata, and also the radio frequency used for the sounding. This is why the layers appear at different depths when we changed frequency and pulse in the vicinity of Dome F (see Fig. 3).

Near MD364 in Figure 3, strata are not clear above 250 m, which suggests that the scattering mechanism might be different above 250 m as compared with deeper regions.

Changes in ΔP_R along the traverse

We assessed the primary causes of the scattering along the traverse in order to better understand the observations at various depths and locations. Figure 4 shows the variation of $\Delta P_R = P_R(179 \text{ MHz}) - P_R(60 \text{ MHz})$ along the traverse for depths of 400, 700 and 1000 m. Since ΔP_R is generally close to 10 dB, Figure 4 indicates that the dominant reflection mechanism at 400 and 700 m is variations in dielectric permittivity, which supports our previous finding (Fujita and others, 1999). At 400 m, ΔP_R is consistently close to 10 dB, with fluctuations of a few dB. These fluctuations are explained by interference between scattering events within a single pulse, so only the average tendency is important. At 700 m, the mean tendency of ΔP_R is a few dB lower. Also, there are fluctuations at the 100–200 km scale. This suggests increased influence from conductivity-based reflections at increasing depths. At 1000 m, ΔP_R is generally close to 0 dB in regions near the dome summit, which means the conductivity-based reflections dominate. At sites >200 km away from the dome, ΔP_R fluctuates between 0 and 10 dB. This suggests that permittivity and conductivity contribute equally to scattering on average, but one or the other dominates in a given region.

DISCUSSION

Causes of stratified scattering

We found that the upper 700 m of the ice sheet is dominated by the stratified changes in permittivity, in agreement with Fujita and others (1999). At 400 m, no effect from electrical conductivity is indicated. Indeed, the ice core at Dome F reveals that fluctuation of the electrical conductivity within the top 700 m is $< 8 \mu\text{S m}^{-1}$. This fluctuation can cause a reflection up to -75 dB at 60 MHz and up to -85 dB at 179 MHz, which cannot be a major cause of the scattering.

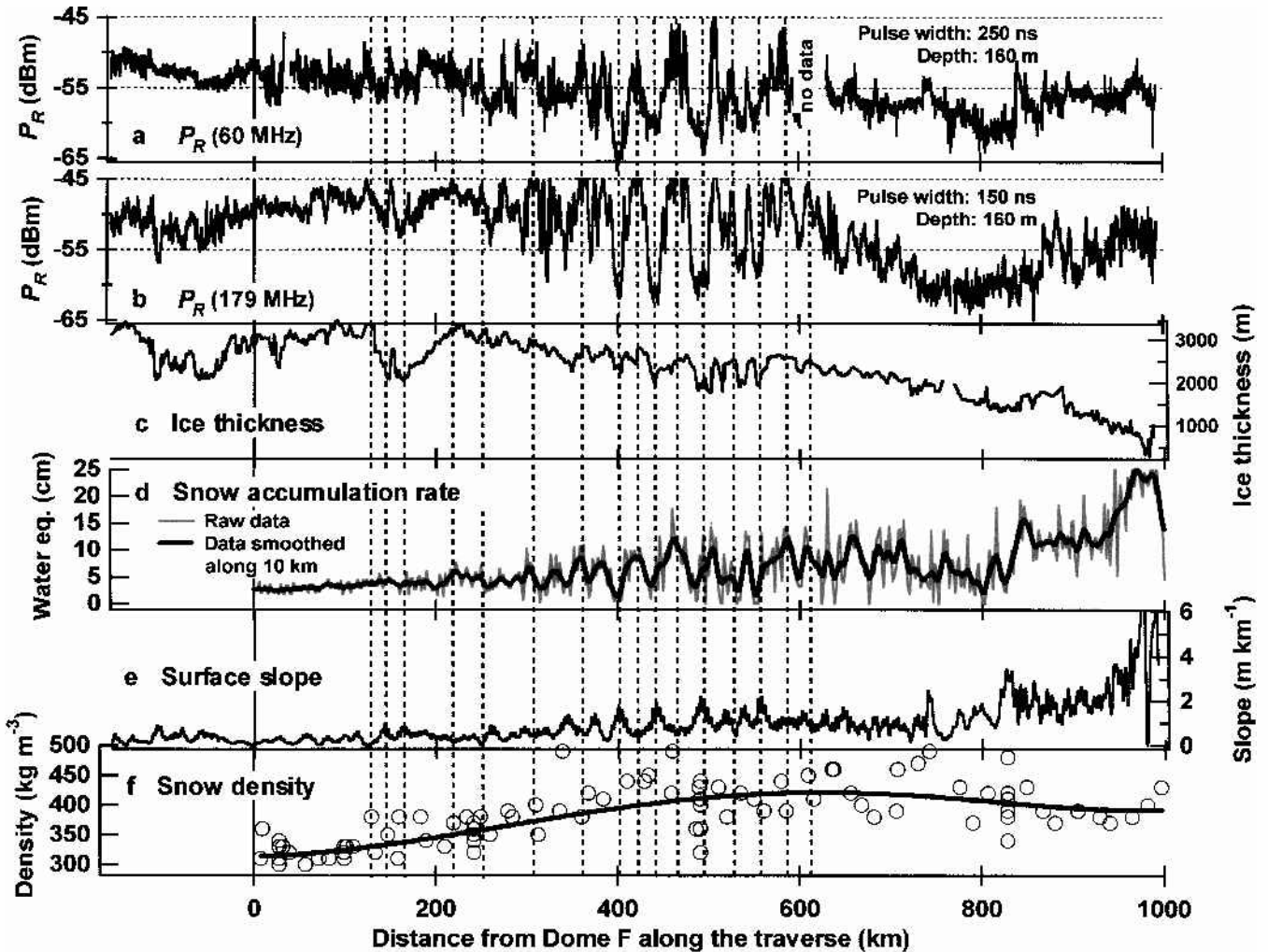


Fig. 5. Radar scattering at 160 m and environmental conditions along the 1150 km traverse. Received power P_R of the 60 MHz radar and the 179 MHz radar scattered from 160 m depth is shown in (a) and (b), respectively. The ice-sheet conditions are as follows: (c) ice thickness; (d) snow accumulation rate (Satow and others, 1999); (e) surface slope along the traverse calculated from the elevation data; (f) density of the snow in the top 20 cm of the ice sheet as measured by a snow sampler and a balance (Azuma and others, 1997; Fujita and others, 1998; Motoyama and others, 1999). The vertical dashed lines indicate the correlations between the profiles. P_R (60 MHz) at sites between SSE150 and Dome F contains a systematic error due to the internal noise of the radar system. It should be a few dB lower.

At 700 m, the conductivity started to have an influence, but permittivity still dominated the scattering. Such changes in permittivity can be caused by fluctuations in either density P_D or crystal-orientation fabrics P_{COF} . P_D might explain all scattering above 700 m because it is known that density changes are caused by trapped air in ice down to depths of 500–1000 m. Below this depth range, the air bubbles change to clathrate hydrate crystals. However, little is presently known about fluctuation of the crystal-orientation fabrics. According to the crystal-orientation analyses for the ice core at Dome F, Azuma and others (2000) discovered that the cluster strength of the c axis around the vertical changed dramatically in many layers within ice from the last glacial age at depths of 500–800 m. It is highly likely that there are similar fluctuations of the crystal-orientation fabrics in many other places along the traverse, and these could cause significant scattering. This role of P_{COF} clearly needs further investigation. When the scattering measurements show strata, the ice layers causing the scattering are very likely from snow accumulation at the same time. Therefore, we assume that these strata are constant time horizons.

Causes and nature of scattering within the top 250 m

Near Dome F, the top 250 m is composed of ice accumulated over the last 7000 years (Figs 2 and 3). At these depths, even our shortest pulse width of 150 ns (13 m in ice) could not detect clear stratification. Within this depth region, however, we measured significant fluctuations of up to 10–15 dB along the traverse (Fig. 5a and b). Here we discuss this shallow scattering.

To understand the physical causes of the P_R signal, various conditions of the ice sheet are compared with P_R in Figure 5. The aim of this comparison is to demonstrate that the electromagnetic scattering from above 250 m in Figure 2 is highly correlated to the environmental conditions of the ice sheet, in particular at the ice-sheet surface. These ice-sheet conditions include ice thickness (Fig. 5c), snow-accumulation rate (Fig. 5d), surface slope along the traverse (Fig. 5e) and density of the snow in the top 20 cm of the ice sheet (Fig. 5f). Of these, ice thickness, snow-accumulation rate and surface slope along the traverse (Fig. 5c–e) are interdependent (Furukawa and others, 1996). A basic

mechanism is that when ice is thick, the vertical flow component of the ice sheet is larger because the same vertical strain rate can cause more vertical displacement at the surface of thicker ice. At the same time, on the relatively flat surface above thicker ice, the snow-accumulation rate is higher because the surface is not eroded by wind compared to more convex surfaces above the subglacial mountains. The higher snow-accumulation rate tends to be shifted to areas where the surface topography is concave. Also, the lower snow-accumulation rate tends to be shifted to the upstream side of the steepest position of each slope.

With the aid of the vertical lines marking locations along the traverse, a correlation rule becomes apparent: (i) where P_R is higher, the ice sheet is thicker than the surroundings, the accumulation rate is higher and the surface slope is lower; similarly, (ii) where P_R is lower, the ice is thinner than the surroundings, the accumulation rate is lower and the surface slope is steeper. Although the magnitudes of the fluctuations are different from one region to another, this rule, with the small phase shift mentioned above, is valid along the traverse line.

The strength of P_R suggests how the density contrasts in the ice sheet distribute from region to region. The electrical conductivity cannot play a role because it is too small (see previous subsection). Also, possible interference effects on the fluctuation of P_R were ruled out because we verified a similar fluctuation of P_R for the two frequencies and three different pulse lengths. The density contrast is higher under the former conditions where P_R is higher, and lower under the latter conditions where P_R is lower. Also, the magnitude of the fluctuations of P_R , 10–15 dB, indicates a density contrast of similar magnitude. Because P_R is generally higher near the dome, the scattering is stronger where strata are more readily formed. Normally, above or slightly upstream of subglacial mountains, the accumulation rate is locally smaller or even has ablation areas, as indicated by a comparison between ice thickness and accumulation rate in Figure 5. The spatially inhomogeneous accumulation rate could explain the low P_R near the surface above the subglacial mountains (Fig. 3). It also explains the low P_R at sites between 600 and 800 km. This region is characterized by low accumulation (Fig. 5d) and the frequent appearance of large sastrugi. Furukawa and others (1996) reported that the maximum frequency distribution of the sastrugi along the same traverse line occurs at sites between 600 and 800 km. According to them, the strong katabatic wind in undulating slopes increased the roughness of the snow surface. In any case, a common feature of the low- P_R sites is the lack of spatially homogeneous accumulation rate. Disturbance in the formation of stratification is characterized by the low accumulation of the snow surfaces exposed to wind erosion above the subglacial mountains and the regions characterized by frequent sastrugi (at 600–800 km). As for the vertical profiles of snow density, Endo and Fujiwara (1973) and Shiraiwa and others (1996) made extensive investigations along the traverse. However, the present data are still insufficient to verify the variability of density deduced from the observation of P_R along the traverse.

For scattering above 250 m, a stratified structure might be measured by using radar pulses narrower than 150 ns (13 m in ice). Indeed, along a 1000 km long traverse in western Dronning Maud Land, Richardson and others (1997) showed that a ground-based snow radar (800–2300 MHz) could detect stratified scattering in snow within the uppermost

12 m. The time resolution of the stratification observed by them was well below 10 ns. This is far below our pulse width, which may be why our very high-frequency data cannot show clear stratification for the scattering shallower than 250 m. To determine if there are strata or if there is some volume scattering without strata, this shallow scattering should be further investigated.

Utilization of scattering for glaciological investigations

Fluctuations of the scattering above 250 m are useful features for glaciological investigations of the ice sheet because they can be used to infer trajectories (particle paths) of the ice flow. Tracing the features of near-vertical white lines in Figure 2 enables trajectories of the ice flow to be identified to depths of about 250 m. Maeno and others (1997) formerly discovered these features at sites 400 km from the dome. The inclination of this feature is shown on the expanded scale of Figure 3b. This feature should have its origin in the accumulation area at a fixed location in the ice sheet above the bedrock where ice is thicker than the surroundings (Maeno and others, 1997). Therefore the locations of the origin do not change with time, and this inclination provides a relation between the horizontal and vertical components of the flow velocity from the origin. In the case of the trajectory at 355 km (indicated by arrow T in Fig. 3), from the surface to 200 m depth the trajectory moved by about 8 km horizontally. Considering the flow velocity measured at MD364 is 4.1 m a^{-1} , the age of the ice at 200 m depth is roughly 2000 years. On the other hand, the annual accumulation rate observed around the 355 km site is 8 cm a^{-1} w.e. Taking into account the densification process of snow to ice, the ice at 200 m depth has a similar age. Therefore, many of the trajectories found in this work (Fig. 2) will similarly provide relations between both vertical and horizontal flow component at these sites. They will be useful for examining ice motion at shallow depths.

In our radar measurements, we could not detect signals shallower than about 100 m since the receiver was switched off to protect it from direct 1 kW transmission signals from the transmitter, and signals larger than -45 dBm were above our upper detection limit. Nevertheless, since strata have their origin at the surface, fluctuations of P_R from strata above 100 m should be detectable. For satellite-borne radars and airborne radars using radio frequencies from MHz to GHz, such scattering fluctuations should be observable because the magnitude is about 5–10 dB for the mean variation and $> 15 \text{ dB}$ for short-scale fluctuations. The backscatter signal of the satellite-borne radar altimeter is an example. Legrésy and Rémy (1997) used the ERS-1 altimeter that used 13 GHz, which has a penetration depth of 10 m, and compiled the magnitude of the backscatter. The backscatter is strongest around Dome F, and decreases away from the dome to the coast by about 5 dB, which is approximately the value we measured. In light of the present study, the distribution of the scattering amplitude should be interpreted in terms of the magnitude of stratified density fluctuations that have their origin as bedrock undulations.

For selection of an ice-coring site for climatic research, stratified layers are very important to ensure that ice cores contain reliable and continuous time series of snow deposition. Disturbance of the layers in Figure 3b and c means that the thickness and the distance of layers change from

place to place. Under such conditions, ice cores can hardly be expected to have a stable and continuous time series of deposition. Therefore, Figure 3a shows that the dome region is an ideal place for ice-core research. We conclude that radar sounding is a valuable means of determining suitable ice-coring locations.

ACKNOWLEDGEMENTS

This paper is a contribution to the Dome Fuji Project, a program conducted by the Japanese Antarctic Research Expedition. The authors thank F. Rémy for making available the edited satellite-based elevation data.

REFERENCES

- Ackley, S. F. and T. E. Kelihier. 1979. Ice sheet internal radio-echo reflections and associated physical property changes with depth. *J. Geophys. Res.*, **84**(B10), 5675–5680.
- Azuma, N. and others. 1997. Glaciological data collected by the 36th Japanese Antarctic Research Expedition during 1995–1996. *JARE Data Rep.* 223.
- Azuma, N. and 6 others. 2000. Crystallographic analysis of the Dome Fuji ice core. In Hondoh, T., ed. *Physics of ice core records*. Sapporo, Hokkaido University Press, 45–61.
- Bogorodsky, V.V., C. R. Bentley and P. E. Gudmandsen. 1985. *Radioglaciology*. Dordrecht, etc., D. Reidel Publishing Co.
- Clough, J. W. 1977. Radio-echo sounding: reflections from internal layers in ice sheets. *J. Glaciol.*, **18**(78), 3–14.
- Endo, Y. and K. Fujiwara. 1973. Characteristics of the snow cover in East Antarctica along the route of the JARE South Pole traverse and factors controlling such characteristics. *JARE Sci. Rep., Ser. C* 7.
- Fujita, S. and S. Mae. 1994. Causes and nature of ice-sheet radio-echo internal reflections estimated from the dielectric properties of ice. *Ann. Glaciol.*, **20**, 80–86.
- Fujita, S., K. Kawada and Y. Fujii. 1998. Glaciological data collected by the 37th Japanese Antarctic Research Expedition during 1996–1997. *JARE Data Rep.*, 234. (Glaciology 27)
- Fujita, S. and 6 others. 1999. Nature of radio-echo layering in the Antarctic ice sheet detected by a two-frequency experiment. *J. Geophys. Res.*, **104**(B6), 13,013–13,024.
- Fujita, S., T. Matsuoka, T. Ishida, K. Matsuoka and S. Mae. 2000. A summary of the complex dielectric permittivity of ice in the megahertz range and its applications for radar sounding of polar ice sheets. In Hondoh, T., ed. *Physics of ice core records*. Sapporo, Hokkaido University Press, 185–212.
- Furukawa, T., K. Kamiyama and H. Maeno. 1996. Snow surface features along the traverse route from the coast to Dome Fuji Station, Queen Maud Land, Antarctica. *Proc. NIPR Symp. Polar Meteorol. Glaciol.* 10, 13–24.
- Gogineni, S., T. Chuah, C. Allen, K. Jezek and R. K. Moore. 1998. An improved coherent radar depth sounder. *J. Glaciol.*, **44**(148), 659–669.
- Gudmandsen, P. 1975. Layer echoes in polar ice sheets. *J. Glaciol.*, **15**(73), 95–101.
- Harrison, C. H. 1973. Radio echo sounding of horizontal layers in ice. *J. Glaciol.*, **12**(66), 383–397.
- Jacobel, R. W. and S. M. Hodge. 1995. Radar internal layers from the Greenland summit. *Geophys. Res. Lett.*, **22**(5), 587–590.
- Legrésy, B. and F. Rémy. 1997. Altimetric observations of surface characteristics of the Antarctic ice sheet. *J. Glaciol.*, **43**(144), 265–275. (Erratum: **43**(145), p. 596.)
- Maeno, H. and 7 others. 1994. Using a mobile radio echo sounder to measure bedrock topography in east Queen Maud Land, Antarctica. *Proc. NIPR Symp. Polar Meteorol. Glaciol.* 8, 149–160.
- Maeno, H., S. Uratsuka, K. Kamiyama, T. Furukawa and O. Watanabe. 1997. [Bedrock topography and internal structures of ice sheet in the Shirase Glacier drainage area revealed from radio-echo soundings.] *Seppyo*, **59**(5), 331–339. [In Japanese with English summary.]
- Matsuoka, K., H. Maeno, S. Uratsuka, S. Fujita, T. Furukawa and O. Watanabe. 2002. A ground-based, multi-frequency ice-penetrating radar system. *Ann. Glaciol.*, **34** (see paper in this volume).
- Millar, D. H. M. 1981. Radio-echo layering in polar ice sheets and past volcanic activity. *Nature*, **292**(5822), 441–443.
- Moore, J. C. 1988. Dielectric variability of a 130 m Antarctic ice core: implications for radar sounding. *Ann. Glaciol.*, **11**, 95–99.
- Motoyama, H. and 8 others. 1995. Preliminary study of ice flow observations along traverse routes from coast to Dome Fuji, East Antarctica by differential GPS method. *Antarct. Rec.*, **39**, 94–98.
- Motoyama, H., Y. Kawamura, M. Kanao, N. Hirasawa, S. Kaneto and T. Yamanouchi. 1999. Glaciological data collected by the 38th Japanese Antarctic Research Expedition during 1997–1998. *JARE Data Rep.* 239. (Glaciology 28)
- Nixdorf, U. and 6 others. 1999. The newly developed airborne radio-echo sounding system of the AWI as a glaciological tool. *Ann. Glaciol.*, **29**, 231–238.
- Parent, J. G. and G. de Q. Robin. 1975. Internal reflections in polar ice sheets. *J. Glaciol.*, **14**(71), 251–259.
- Richardson, C., E. Aarholt, S.-E. Hamran, P. Holmlund and E. Isaksson. 1997. Spatial distribution of snow in western Dronning Maud Land, East Antarctica, mapped by a ground-based snow radar. *J. Geophys. Res.*, **102**(B9), 20,343–20,353.
- Robin, G. de Q. and D. H. M. Millar. 1982. Flow of ice sheets in the vicinity of subglacial peaks. *Ann. Glaciol.*, **3**, 290–294.
- Robin, G. de Q., S. Evans and J. T. Bailey. 1969. Interpretation of radio echo sounding in polar ice sheets. *Philos. Trans. R. Soc. London, Ser. A*, **265**(1166), 437–505.
- Satow, K., O. Watanabe, H. Shoji and H. Motoyama. 1999. The relationship among accumulation rate, stable isotope ratio and surface temperature on the plateau of east Dronning Maud Land, Antarctica. *Polar Meteorol. Glaciol.* 13, 43–52.
- Shiraiwa, T., H. Shoji, T. Saito, K. Yokoyama and O. Watanabe. 1996. Structure and dielectric properties of surface snow along the traverse route from coast to Dome Fuji Station, Queen Maud Land, Antarctica. *Proc. NIPR Symp. Polar Meteorol. Glaciol.* 10, 1–12.
- Uratsuka, S., H. Maeno, T. Suitz and D. A. Fisher. 2000. Development and field experiment of L-band high-resolution ice-radar. *IEICE Trans. Commun.*, **E83B**(9), 1969–1977.
- Watanabe, O. and 16 others. 1999. Basic analyses of Dome Fuji deep ice core. Part I: stable oxygen and hydrogen isotope ratios, major chemical compositions and dust concentration. *Polar Meteorol. Glaciol.*, **13**, 83–89.